PHYSICAL REVIEW C **75**, 054321 (2007)

First identification of excited states in ^{169}Ir

M. Sandzelius,[1,*] C. Scholey,[2] B. Cederwall,[1] E. Ganioğlu,[3,†] K. Andgren,[1] D. E. Appelbe,[4] C. J. Barton,[4,‡] T. Bäck,[1] S. Eeckhaudt,[2,§] T. Grahn,[2,∥] P. T. Greenlees,[2] B. Hadinia,[1] A. Johnson,[1] P. M. Jones,[2] D. T. Joss,[3,∥] R. Julin,[2] S. Juutinen,[2] H. Kettunen,[2] K. Lagergren,[1,¶] M. Leino,[2] A.-P. Leppänen,[2] P. Nieminen,[2,**] R. D. Page,[5] J. Pakarinen,[2,∥] J. Perkowski,[2,††] P. Rahkila,[2] J. Simpson,[4] J. Uusitalo,[2] K. Van de Vel,[2,§] D. D. Warner,[4] D. R. Wiseman,[5] and R. Wyss[1]

[1] *Department of Physics, Royal Institute of Technology, SE-10691 Stockholm, Sweden*
[2] *Department of Physics, University of Jyväskylä, P.O. Box 35 (YFL), FIN-40014 Jyväskylä, Finland*
[3] *Science Faculty, Physics Department, Istanbul University, TR-34459 Istanbul, Turkey*
[4] *CCLRC, Daresbury Laboratory, Daresbury, Warrington WA4 4AD, United Kingdom*
[5] *Oliver Lodge Laboratory, Department of Physics, University of Liverpool, Liverpool L69 7ZE, United Kingdom*

(Received 7 February 2007; published 17 May 2007)

Gamma rays populating the α-decaying isomeric state in ^{169}Ir have been observed for the first time. The experiment employed the recoil-decay tagging method using the JUROGAM γ-ray spectrometer, the RITU gas-filled recoil separator and the GREAT spectrometer located at the RITU focal plane. The γ-ray cascade feeding the isomeric α-decaying state exhibits a rotational structure consistent with a $h_{11/2}$ proton coupled to a triaxially deformed core. The experimental results are compared with predictions from total Routhian surface calculations.

DOI: 10.1103/PhysRevC.75.054321 PACS number(s): 27.70.+q, 21.10.Re, 23.20.Lv, 23.60.+e

I. INTRODUCTION

Neutron-deficient iridium isotopes lie between the deformed rare-earth nuclei and the near spherical closed proton shell at $Z = 82$. Many of these nuclei are known to exhibit collective structures reflecting a variety of shapes and shape coexistence. Shape coexistence is well known for low-lying spherical, oblate, triaxial and prolate deformed states in the chains of neutron deficient isotopes near the $Z = 82$ shell closure where proton 2p-2h excitations are important [1]. As the $N = 82$ shell gap is approached from the neutron midshell ($N = 104$) the positions of the proton and neutron Fermi surfaces relative to the N, $Z = 82$ shell gaps make the nuclear potential soft with respect to elongation (β_2) and triaxiality (γ). A "classic" example of shape coexistence is the structure of the ground-state band in ^{176}Pt [2,3], which in experiment was found to exhibit peculiar features. These features were interpreted as resulting from coexistence between a weakly deformed triaxial structure and a moderately deformed prolate intruder configuration. Similar behavior can be found in neighboring neutron-deficient $_{78}$Pt and $_{76}$Os [4–6] isotopes where intruder states create mixed configurations at the Fermi surface, resulting in well-deformed states coexisting with less deformed, triaxial states. With decreasing neutron number weakly deformed triaxial shapes are increasingly favored while the more deformed prolate states are pushed upward in energy, at least at low spins.

Odd-A nuclei are of key interest for studies of nuclear shapes since the coupling of the odd particle to the deformed even-even core can lead to shape dependent effects on the rotational spectra and their electromagnetic properties, hence serving as a probe of the nuclear shape. Depending on the nature and magnitude of the nuclear deformation, different single-particle configurations are favored and their relative energies, therefore also contain information on the nuclear shape. Furthermore, the shape-polarizing effects of individual single-particle orbitals can reveal important clues for understanding the mechanisms behind the onset of collectivity and deformation near closed shells. Shape-polarization effects are generally believed to be associated with two-particle two-hole (2p-2h) excitations across a major shell gap and/or with the occupation of specific shape-driving orbitals such as the high-j unique parity (intruder) levels.

For the odd-even nuclei in this mass region, valence protons occupying either the $s_{1/2}$, $d_{3/2}$, or $h_{11/2}$ orbitals dominate the structure at low spin and low excitation energy. Two low-lying states are generally observed to decay by proton, α or β emission. Depending on Z, these states are usually associated with either an unpaired $s_{1/2}$ or $h_{11/2}$ proton, with the $s_{1/2}$ configuration forming the ground state [7]. Since γ-ray transitions between these states would be very slow due to the large spin difference, charged particle emission is the dominating decay mode for these states.

---

[*] Corresponding author. Email address: sandzelius@nuclear.kth.se

[†] Also at: Department of Physics, Royal Institute of Technology, SE-10691 Stockholm, Sweden.

[‡] Present address: Department of Physics, University of York, York, Heslington YO1 5DD, UK.

[§] Also at: Instituut voor Kern-en Stralingsfysica, Departement of Physics, University of Leuven, Celestijnenlaan 200D, B-3001 Leuven, Belgium.

[∥] Present address: Oliver Lodge Laboratory, Department of Physics, University of Liverpool, Liverpool L69 7ZE, UK.

[¶] Present address: Joint Institute for Heavy Ion Research, Holifield Radioactive Ion Beam Facility, Oak Ridge, TN-37831, USA.

[**] Present address: Australian National University, Canberra, ACT 0200, Australia.

[††] Also at: Department of Nuclear Physics, Radiation Safety, University of Lodz, Pomorska, 149/153, PL-90-236, Lodz, Poland.

The heaviest neutron-deficient $^{187-189}$Ir isotopes show signs of triaxiality and γ softness [8,9], which disappear near the neutron midshell ($N = 104$) where prolate structures become more prominent. From ^{173}Ir to ^{181}Ir rotational bands consistent with configurations based on $h_{11/2}$, $h_{9/2}$, and $i_{13/2}$ orbitals of prolate shape have been observed up to high spins [10–14]. In the lightest odd-mass isotopes, $^{171-175}$Ir, triaxiality again is an important feature as the yrast bands show increasing signature splitting with decreasing neutron number. In this transitional region with $N < 96$ it has been suggested that a change from a triaxial shape at low spin to a prolate deformation at higher spins could be taking place in the $h_{11/2}$ bands [10–12,15]. Two α-decaying states have previously been assigned to ^{169}Ir and their properties examined by Poli *et al.* [16]. The strongest α-decay branch was suggested to depopulate an isomeric state based on the $h_{11/2}$ configuration and the weaker ground-state α-decay branch was assigned to emanate from an $s_{1/2}$ configuration. Both the isomeric and ground-state α decays were identified and confirmed in this work, and an excited structure is found to be based on the isomeric $h_{11/2}$ state.

II. EXPERIMENTAL DETAILS

The experiment was performed at the Accelerator Laboratory of the University of Jyväskylä employing the K130 cyclotron. Excited states in ^{169}Ir were populated using the ^{112}Sn(^{60}Ni, $p2n$) reaction at a bombarding energy of 266 MeV. The ^{112}Sn target consited of two stacked self-supporting foils of a total thickness of 800 μg/cm^2 and with ~93% isotopic enrichment. The average beam intensity was 4.7 pnA during 6 days of irradiation time. Prompt γ rays were detected at the target position by the JUROGAM array consisting of 43 EUROGAM phase I [17] and GASP [18] type Compton-suppressed high-purity germanium detectors. The germanium detectors were distributed in six rings at six different angles relative to the beam direction, with five detectors at 158°, ten at 134°, ten at 108°, five at 94°, five at 86°, and eight at 72°. In this configuration JUROGAM had a total photopeak efficiency of 4.2% at 1.3 MeV.

Fusion-evaporation products were separated in-flight from fission products and scattered beam particles using the RITU gas-filled recoil separator [19,20] and subsequently implanted at the focal plane into the double-sided silicon strip detectors (DSSD) of the GREAT spectrometer. The GREAT [21] spectrometer is a composite detector system, which in addition to the two DSSDs, comprises a multiwire proportional counter (MWPC), an array of 28 Si PIN diode detectors and two segmented germanium detectors. Each DSSD has an effective area of $60 \times 40\,\mathrm{mm}^2$, with 200 individual strips at a pitch of 1mm in both directions leading to 4800 independent pixels in total. All detector signals were recorded independently by the triggerless total data readout (TDR) acquisition system [22] where they were given a time stamp of 10 ns precision. This allowed for accurate temporal correlations between prompt γ rays detected at the target position, recoil implants at the RITU focal plane and their subsequent radioactive decays to be performed. Spatial and temporal correlations in the recorded data were analysed on and off-line using the GRAIN software package [23].

Clean γ-ray spectra were obtained using the highly selective recoil decay tagging technique (RDT) [24,25]. An α decay detected at the same position (pixel) as a previously implanted recoiling residue provided identification for the residue using its characteristic energy and decay time of the α decay. Prompt γ rays at the target position could then be associated with the implantation event. In the case of ^{169}Ir the relatively short α-decay half-life previously measured to be 323^{+90}_{-66} ms for the isomeric state [16], ensured that the selection was clean with respect to random correlations, since the beam intensity was kept low in order to minimise the probability that a second recoiling residue would strike the same pixel in the DSSD before the former had time to α decay. The average count rate of the DSSD was ~350 Hz.

III. EXPERIMENTAL RESULTS

The reaction employed in this experiment was primarily used to study the $2n$ fusion-evaporation channel populating the neutron-deficient nucleus ^{170}Pt [26]. In this work we present data for the $p2n$ exit channel leading to ^{169}Ir with a cross section of $\sigma \sim 120\,\mu$b. Two α-decaying states were identified. The more strongly populated α-decaying state is an isomeric state with measured decay energy of $E_\alpha = 6117(3)$ keV and a measured half-life of $t_{1/2} = 280(3)$ ms. The second α-decaying state is thought to be the more weakly populated ground state with measured decay energy of $E_\alpha = 6010(8)$ keV. No accurate half-life could be extracted for the ground-state α decay since the decay spectrum was too contaminated with stronger competing channels with overlapping decay properties. The low-lying isomeric state is 153(24) keV above the ground state as established by Poli *et al.* [16] who studied extended α-decay chains starting from the ground and isomeric state decays of ^{177}Tl. In that work, the observation of proton decays of ^{177}Tl allowed the ground state to be assigned to a $s_{1/2}$ configuration and the isomeric state to a $h_{11/2}$ configuration. The γ-ray spectra correlated with the isomeric α decay in ^{169}Ir and the corresponding daughter α decay are shown in Fig. 1. The γ-ray energies, relative intensities, angular distribution ratios (R), and level spin assignments from the decays of excited states built on the $h_{11/2}$ isomeric state of ^{169}Ir are listed in Table I.

The results for the structure feeding the isomeric $h_{11/2}$ state for ^{169}Ir were obtained from γ-γ coincidence events correlated with its α decay [$E_\alpha = 6117(3)$ keV, $t_{1/2} = 280(3)$ ms] detected within 900 ms of a recoil implantation in the same DSSD pixel. The data were sorted into a $E_{\gamma1}$-$E_{\gamma2}$ coincidence matrix and analysed using the GRAIN [23] and RADWARE [27] software packages. The ^{169}Ir γ-γ matrix contained 2.16×10^5 pairs of γ rays. Since the neighboring isotope ^{170}Ir was populated via the pn-channel and has a similar α-decay energy to ^{169}Ir [$E_\alpha(^{170}\mathrm{Ir}) = 6083(11)$ keV and $t_{1/2} = 830(300)$ ms [7], there was some contamination from ^{170}Ir in the α-tagged ^{169}Ir γ-ray spectrum. Figure 1(a) shows a spectrum of γ rays emitted during the deexcitation of excited states within ^{169}Ir which is visibly contaminated by the three strongest

TABLE I. Gamma rays assigned to ^{169}Ir that were observed to populate the isomeric $h_{11/2}$ state. Intensities (I_γ) are adjusted for detector efficiencies and normalised to the strongest transition at $E_\gamma = 658$ keV (statistical uncertainties are given in parentheses). Transitions marked with an asterisk are assigned to ^{169}Ir but not placed into the level scheme.

E_γ (keV)	I_γ(%)	R	$J_i^\pi \to J_f^\pi$
101.4(1)*	6.1(5)		
121.1(1)*	6.6(5)		
130.5(1)	24.3(7)		$(25/2^-) \to (23/2^-)$
152.3(1)	23.6(7)		$19/2^- \to 19/2^-$
159.5(2)	16.4(6)		$(27/2^-) \to (25/2^-)$
178.0(3)	12.0(5)		$19/2^- \to 17/2^-$
190.6(3)*	5.5(4)		
201.7(3)	31.5(8)	0.76(3)	$15/2^- \to 13/2^-$
206.5(1)	14.3(6)		$(23/2^-) \to (21/2^-)$
223.6(2)	17.0(6)		$23/2^- \to 21/2^-$
232.5(4)*	2.7(4)		
242.5(4)[a]	26.8(7)	0.67(2)	$19/2^- \to 17/2^-$
252.9(6)	14.0(5)		$(29/2^-) \to (27/2^-)$
256.6(4)[b]	28.0(8)		$(19/2^-) \to 17/2^-$
263.8(2)	4.7(5)		$(21/2^-) \to 21/2^-$
273.9(3)[c]	62.6(11)	0.87(3)	$21/2^- \to 19/2^-$
290.6(3)	<2.0[d]		$23/2^- \to 21/2^-$
310.6(2)	5.8(5)		$(25/2^-) \to (23/2^-)$
317.6(4)	24.5(7)		$(23/2^-) \to 21/2^-$
323.6(2)	7.7(4)		$(33/2^-) \to (31/2^-)$
328.6(1)*	7.3(4)		
335.1(2)*	6.5(4)		
341.2(2)*	4.1(4)		
353.2(2)*	8.0(4)		
361.0(2)*	5.2(4)		
383.7(2)	5.6(7)		$(25/2^-) \to (23/2^-)$
393.3(1)	40.7(9)	0.64(7)	$19/2^- \to 17/2^-$
457.1(2)	96.5(12)	0.92(2)	$13/2^- \to 11/2^-$
497.0(3)*	5.7(4)		
515.1(3)	5.8(21)		$(23/2^-) \to (19/2^-)$
519.3(4)	46.6(10)	0.89(2)	$17/2^- \to 15/2^-$
539.2(1)	18.4(8)		$(23/2^-) \to 19/2^-$
542.8(1)	8.1(8)		$21/2^- \to 19/2^-$
559.9(2)	6.4(9)		$(17/2^-) \to (15/2^-)$
601.8(2)*	11.1(9)		
610.5(3)*	5.3(10)		
633.1(2)	13.6(6)		$(15/2^-) \to 13/2^-$
658.3(3)	100.0(13)	1.15(2)	$15/2^- \to 11/2^-$
688.4(1)	19.0(6)		$(21/2^-) \to 19/2^-$
720.3(2)	29.6(9)	1.29(5)	$17/2^- \to 13/2^-$
745.4(2)	12.4(7)		$(23/2^-) \to 19/2^-$
762.4(4)	47.6(10)	1.26(10)	$19/2^- \to 15/2^-$
785.3(2)	6.7(5)	1.42(10)	$21/2^- \to 17/2^-$
833.5(4)	11.0(5)		$23/2^- \to 19/2^-$
937.3(3)	19.6(7)		$17/2^- \to 13/2^-$
992.5(2)	9.9(6)		$(19/2^-) \to 15/2^-$

[a] Two transitions separated by ~1 keV where the intensity is shared between the 242 and 243 keV transitions.

[b] The 257 keV transition is a self-coincident doublet.

[c] Two unresolved transitions at 273 and 274 keV. The bulk of the intensity is carried by the 274 transition.

[d] Too weak to extract an accurate intensity.

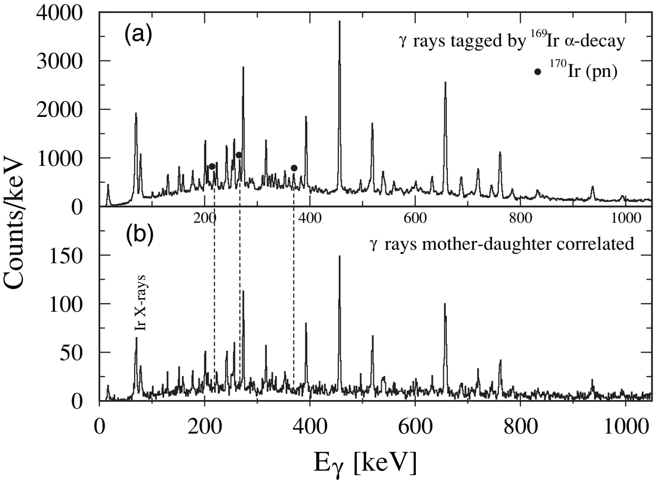

FIG. 1. (a) Recoil-α correlated ^{169}Ir γ-ray spectrum. Lines marked with a dot represent contamination from the three strongest transitions in ^{170}Ir, at 218, 267 and 370 keV, respectively [28]. (b) As in (a), but requiring additional correlation with the isomeric ($h_{11/2}$) ^{165}Re daughter α decay [7].

^{170}Ir γ-ray transitions [28]. This contamination is largely removed in the mother-daughter correlated γ-ray spectrum shown in Fig. 1(b). Although the α-decay properties are very similar in the daughter nuclei of ^{169}Ir and ^{170}Ir, with $E_\alpha(^{165}\text{Re}) = 5518(5)$ keV, $t_{1/2}(^{165}\text{Re}) = 1.9(3)$ s and $E_\alpha(^{166}\text{Re}) = 5533(10)$ keV, $t_{1/2}(^{166}\text{Re}) = 2.1(4)$ s [7], the mother-daughter correlated spectrum shows unambiguous γ-ray identification of ^{169}Ir due to the much weaker α-decay branch in ^{166}Re compared with that in ^{165}Re.

The partial level scheme for ^{169}Ir deduced from the γ-γ matrix tagged by the isomeric α-decay is shown in Fig. 2. Several other α-tagged ^{169}Ir γ rays were identified (see Table I), but either poor statistics or ambiguous coincidence relationships prevented them from being firmly placed in the level scheme. The yrast γ-ray cascade is here assigned to be built on the $\pi h_{11/2}$ state and the γ-ray emission is followed by the subsequent 6117(3) keV α decay of this state. This state

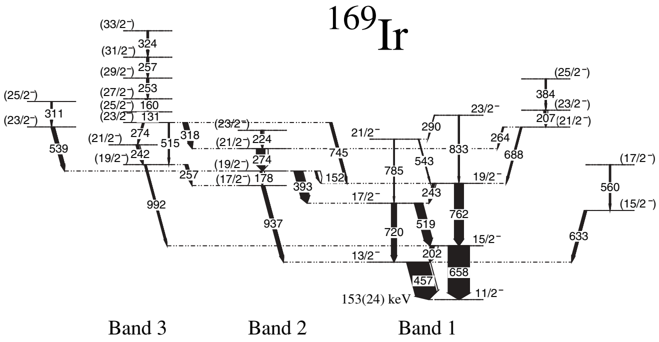

FIG. 2. Level scheme for ^{169}Ir as deduced in the present work. Gamma rays are labeled with transition energies in keV. The intensity of the transitions is proportional to the width of the arrows. Tentative spin and parity assignments are indicated by parentheses. The isomeric $h_{11/2}$ band head is at 153(24) keV above the $s_{1/2}$ ground state [16] (not shown in the level scheme).

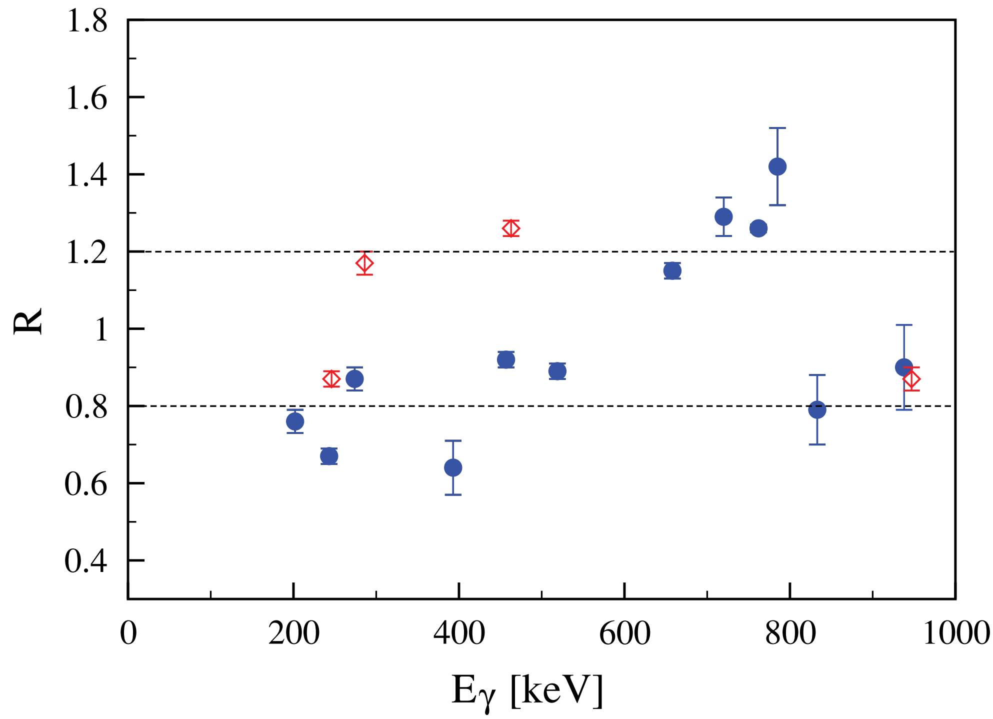

FIG. 3. (Color online) Angular intensity ratios as a function of γ-ray transition energy in ^{169}Ir (filled circles) defined through Eq. (1). Diamonds represent reference values for stretched $E2$ (286 keV and 463 keV) transitions in ^{170}Os and stretched $M1$ and $E1$ (246 keV and 947 keV) transitions in ^{169}Re and ^{170}Os, respectively.

is situated at an excitation energy of 153(24) keV above the α-decaying ground state [16]. The level scheme has a very similar structure to that of ^{171}Ir, which also was assigned to be built on a $\pi h_{11/2}$ state [15]. The spin and parity assignments in the level scheme follow the assumption of a $11/2^-$ band head, which is expected near the Fermi surface. Configuration assignments are discussed in more detail in Sec. IV. In all, 37 γ-ray transitions were placed into the level scheme, which reaches an excitation energy of $E_x = 3439(24)$ keV above the $s_{1/2}$ ground state and a tentative spin and parity $I^\pi = 33/2^-$. The yrast sequence at low spins in ^{169}Ir (labeled as Band 1 in Fig. 2) forms a coupled band structure that extends to spin $I^\pi = 23/2^-$ at an excitation energy of $E_x = 2406(24)$ keV above the $s_{1/2}$ ground state. It consists of in-band $E2$ transitions together with $M1$ crossover transitions. The placement of the transitions is based on relative γ-ray intensities and γ-γ coincidence relationships.

Multipolarity assignments for Band 1 and for some of the strongest γ-ray transitions feeding into this band were obtained from intensity ratios considering γ rays measured at $\Theta = 158^\circ$ and $\Theta = 86^\circ$ and 94° angles relative to the beam direction in the JUROGAM spectrometer. These angular distribution ratios are calculated through the relation

$$R = N\left[\frac{I_\gamma(158^\circ)}{I_\gamma(86^\circ) + I_\gamma(94^\circ)}\right], \tag{1}$$

where N is a normalization constant to account for the different number of detectors; in this case $N = 2$. In order to obtain typical values of stretched quadrupole and stretched dipole transitions, the R values were compared to those of γ rays previously assigned to some of the stronger evaporation channels in the experiment. The R values measured were 1.26(2) for the $4^+ \rightarrow 2^+$ 463 keV transition in ^{170}Os [29] and 0.87(6) for the $13/2^- \rightarrow 11/2^-$246 keV transition in ^{169}Re [30], respectively. Therefore, assignment of stretched quadrupole and stretched dipole transitions in ^{169}Ir were made for anisotropies around 1.2 and 0.8, respectively (see Table I and Fig. 3).

Two side structures (labeled Band 2 and Band 3 in Fig. 2) have been identified. Both of these bands feed into the yrast band, with most of the intensity in Band 2 flowing through the 393 keV and 937 keV transitions, populating states in Band 1 at $17/2^-$ and $13/2^-$. The 393 keV transition shows an anisotropy consistent with a dipole transition and is therefore interpreted as a $\Delta I = 1$ transition depopulating a $I^\pi = 19/2^-$ state. Although tentative, this, together with the relative intensities of the γ rays depopulating, e.g., the $(19/2^-)$ state of Band 2, is consistent with the proposed spin and parity assignments of the states in Band 2. A γ-ray coincidence spectrum produced by putting a gate on the 393 keV transition is shown in Fig. 4(a). It shows members of Band 2 and in addition, although weakly, transitions associated with Band 3. The reason for the relative weakness of transitions in Band 3 in this gate is that a large fraction of the intensity bypasses the 393 keV transition via the 745 and 992 keV transitions. Although the in-band transitions of Band 3 can be placed in the level scheme by their relative intensities and coincidence relationships firm multipolarity assignments using angular distribution ratios are not possible due to insufficient statistics. Therefore these spin and parity assignments are tentative.

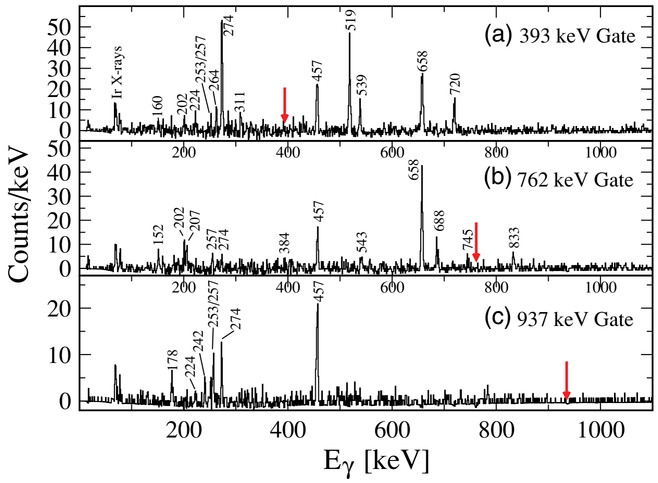

FIG. 4. (Color online) Three γ-γ coincidence spectra generated from the recoil-α tagged ($E_\alpha = 6117$ keV) $E_{\gamma 1}$-$E_{\gamma 2}$ coincidence matrix. The three gates, indicated by arrows, demonstrate the most salient features of the ^{169}Ir level scheme: (a) spectrum in coincidence with the 393 keV transition depopuling Band 2, (b) spectrum in coincidence with the 762 keV transition in Band 1, and (c) spectrum in coincidence with the 937 keV transition connecting Band 2 with Band 1.

Gating on the 762 keV transition in the yrast coupled band structure [see Fig. 4(b)] reveals, in addition to all its members, an additional structure feeding into Band 1 via the 688 keV and Band 2 via the 264 keV transition, respectively. Spin and parity assignments for these side bands feeding into the ground state band are tentative.

IV. DISCUSSION

The yrast band (Band 1) in ^{169}Ir is interpreted as a deformed one-quasiparticle configuration primarily based on the $\frac{11}{2}^-[505]$ Nilsson state originating from the $\pi h_{11/2}$ spherical subshell. ^{169}Ir does not have multiple rotational bands, unlike in heavier ($A \geqslant 171$) odd-mass iridium nuclei, for which additional $\frac{5}{2}^+[402]$ and $\frac{1}{2}^-[541]$ band heads are found at low excitation energies with the $\frac{1}{2}^-[541]$ Nilsson state forming the ground state. In $^{173-175}$Ir, structures built on the $\frac{1}{2}^+[660]$ orbital of $i_{13/2}$ parentage are also observed as intruder bands of large prolate deformation [10,11]. Furthermore, in ^{169}Ir the $\frac{11}{2}^-[505]$ band quickly becomes unfavored, i.e., nonyrast (see Fig. 2), and does not extend to high enough spin for the expected $i_{13/2}$ neutron alignment to be observed.

In order to interpret the structures of the extremely neutron deficient odd-A isotopes, and in particular that of ^{169}Ir, we have performed total Routhian surface (TRS) calculations [31]. For each rotational frequency, the total energy in the rotating frame (Routhian) is minimized as a function of the deformation parameters β_2 and γ. Figure 5 displays the calculated TRSs for the lowest negative parity, negative signature configuration (corresponding to the $\alpha = -1/2$ branch of Band 1) for ^{169,171,173}Ir at a rotational frequency of $\hbar\omega = 0.16$ MeV. In order to illustrate the effect of the odd proton on the nuclear deformation, the vacuum configurations for the corresponding Pt and Os isotones are also shown. Table II displays the relevant deformation parameters (γ and β_2) for the three Pt-Ir-Os isotones shown in Fig. 5. The deformation parameters correspond to the most favored collective energy minima of the TRSs. The TRS plot for ^{169}Ir in Fig. 5 shows a minimum at

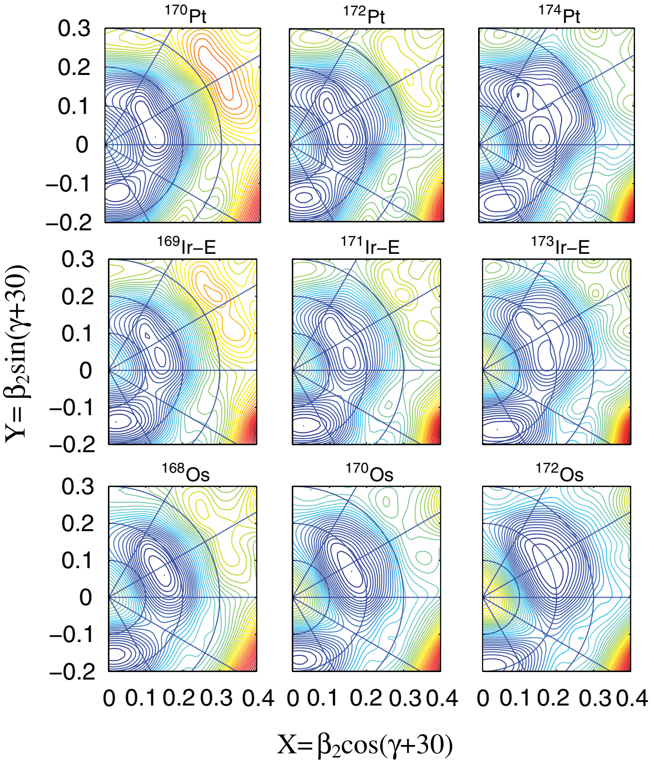

FIG. 5. (Color online) Calculated TRSs for the even-N Pt-Ir-Os $N = 92$–96 isotones showing the total energy in the rotating frame as a function of the deformation parameters γ and β_2 at a rotational frequency $\hbar\omega = 0.16$ MeV. The top panels show the even-even $^{170-174}$Pt isotopes. The middle panels show the $(\pi, \alpha) = (-, -1/2)$ configuration of the odd-A $^{169-173}$Ir isotopes and the bottom panels display the even-even $^{168-172}$Os isotopes. The energy difference between contour lines is 100 keV.

TABLE II. Calculated deformation parameters γ and β_2 for the Pt-Ir-Os isotopes in Fig. 5 for the $(\pi, \alpha) = (-, -1/2)$ configuration at $\hbar\omega = 0.16$ MeV.

Isotope			γ	β_2
$N = 92$	$N = 94$	$N = 96$		
^{170}Pt			-21°	0.13
^{169}Ir			-16°	0.14
^{168}Os			-5°	0.16
	^{172}Pt		-23°	0.15
	^{171}Ir		-20°	0.16
	^{170}Os		-9°	0.17
		^{174}Pt	-24°	0.16
		^{173}Ir	-23°	0.17
		^{172}Os	-12°	0.20

a triaxial deformation of $\beta_2 \simeq 0.14$ and $\gamma = \pm 16^\circ$. However, the nucleus demonstrates pronounced γ softness indicating that only a small increase in energy may easily change the sign of the γ deformation to either extreme, in this case from $\gamma \approx 16^\circ$ to $\gamma \approx -16^\circ$ with increasing rotational frequency, since at higher rotational frequencies a negative γ deformation is favored over a positive γ deformation. The energy minimum in the lowest negative-parity TRS of ^{169}Ir is assigned to the one-proton $\pi h_{11/2}[505]\frac{11}{2}^-$ configuration following the argument in [32,33]. Another minimum becomes visible with increasing rotation and appears at a deformation around $\beta_2 \approx 0.15$ and $\gamma \approx -105^\circ$. This minimum is lower in energy but is noncollective, and it might be associated with one of the other band structures observed in ^{169}Ir.

As can be seen in Fig. 5 and Table II, the position of the proton Fermi level is predicted to significantly influence the tendency toward triaxiality of the even-even core. The addition of the high-j proton to ^{168}Os drives the core from an almost axially (albeit γ-soft) symmetric shape to one with a more pronounced γ deformation. When adding two protons to the ^{168}Os core the resulting TR surface for ^{170}Pt reveals an even larger degree of triaxiality than the ^{169}Ir ($\pi = -1, \alpha = -1/2$) configuration. The predicted trend of increasing γ deformation as a function of increasing proton number is coupled to a parallel tendency toward smaller β_2 deformation. However, while there is a large increase in γ deformation between $Z = 76$ and $Z = 78$, the triaxial minimum based on the $h_{11/2}$ configuration for ^{169}Ir is deeper than that of ^{170}Pt. Hence, a shape polarizing effect can be inferred for the odd $h_{11/2}$ proton as well. A different shape dependence with the neutron number is predicted: Increasing the neutron number results in an increase in both γ and β_2 deformation.

TRS plots for the ($\pi = +, \alpha = +1/2$) configuration of ^{169}Ir are shown in Fig. 6 for $\hbar\omega = 0$ and $\hbar\omega = 0.160$ MeV. The TRS calculation predicts a deformation $\beta_2 \approx 0.15$ and $\gamma \approx -16^\circ$ for this configuration. The deformation of the ground state is thus very similar to that of the isomeric $h_{11/2}$ state. This is the lowest single-proton configuration in ^{169}Ir and corresponds to a mixed ($d_{3/2}, s_{1/2}$) ground state.

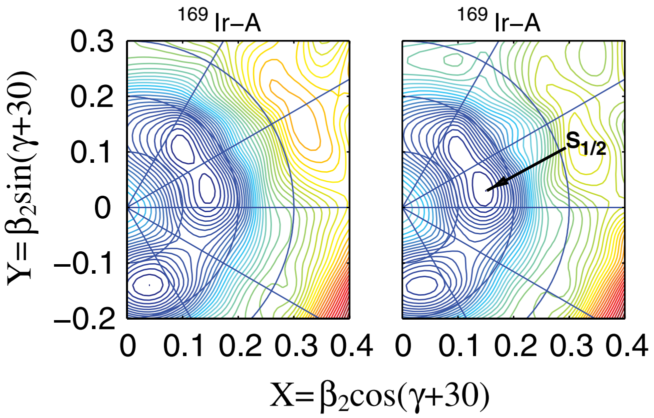

FIG. 6. (Color online) Calculated TRSs for the $(\pi, \alpha) = (+, +1/2)$ A-configuration of ^{169}Ir showing deformation parameters γ and β_2 at rotational frequency $\hbar\omega = 0.0$ (left panel) and $\hbar\omega = 0.16$ MeV (right panel). The energy difference between contour lines is 100 keV.

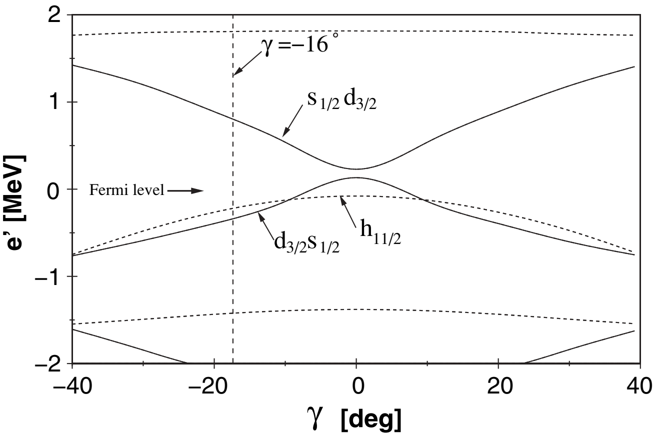

FIG. 7. Proton single-particle levels (e') as a function of the triaxiality parameter γ. The single-particle levels are labeled with their spherical subshell origin as described in the text. The plot is made with $\beta_2 = 0.142$ and $\hbar\omega = 0.0$ MeV, using a universal Woods-Saxon potential. The solid lines show levels with $(\pi, \alpha) = (+, +1/2)$ and $(+, -1/2)$, and the dashed lines those of $(\pi, \alpha) = (-, +1/2)$ and $(-, -1/2)$. The vertical dashed line indicate the relevant γ deformation for ^{169}Ir.

In order to elucidate the triaxial shape-driving properties of different proton configurations in ^{169}Ir, Fig. 7 shows the calculated single-particle levels (labeled by the corresponding spherical subshell) as a function of the triaxiality parameter, γ. The $\frac{11}{2}^-[505]$ proton orbital originating from the $h_{11/2}$ subshell is energetically favored by an increase in γ deformation. However, the slope is rather small, indicating that its shape polarizing effect is limited. From Fig. 7 it is also clear that the mixed ($d_{3/2}, s_{1/2}$) ground state, formed by the Nilsson $\frac{1}{2}^+[400]$ and $\frac{3}{2}^+[402]$ orbitals, is indeed lower in energy than the isomeric orbital $\frac{11}{2}^-[505]$ from the $h_{11/2}$ spherical subshell at the relevant γ deformation of -16°. This prediction is in agreement with the experimental result where the isomeric $h_{11/2}$ state is situated at an excitation energy of ~150 keV above the $s_{1/2}$ ground state. This interpretation is also consistent with the full TRS calculation where the lowest minimum for the $h_{11/2}$ state is situated ~30 keV above the lowest minimum for the $s_{1/2}$ ground state. However, cranked shell model calculations show that at this γ deformation the ground state is an approximately equal mixture of the states emanating from the $s_{1/2}$ and $d_{3/2}$ spherical subshells.

The observed $h_{11/2}$ band in ^{169}Ir shows a large signature splitting of $\simeq$150 keV at low spins. This signature splitting is compared in Fig. 8 with that of the corresponding bands in the heavier iridium isotopes ^{171}Ir [15], ^{173}Ir [10], and ^{175}Ir [11], using the staggering parameter S(I) [34] defined as

$$S(I) = E(I) - E(I-1) - \tfrac{1}{2}[E(I+1) - E(I) + E(I-1) - E(I-2)]. \qquad (2)$$

The signature splitting in ^{169}Ir indicates a triaxial deformation ($\gamma < 0$) and is expected to arise from the influence on the

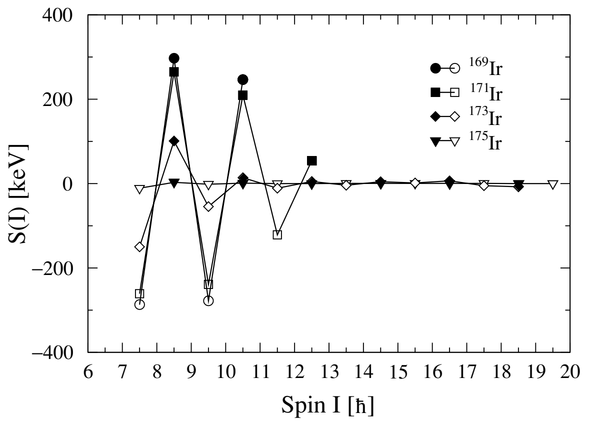

FIG. 8. Staggering parameter S(I) as a function of spin I for the [505]11/2$^-$ bands in the neutron-deficient odd-A iridium isotopes $^{169-175}$Ir. The filled (open) symbols represent the $\alpha = +1/2$ ($\alpha = -1/2$) signature.

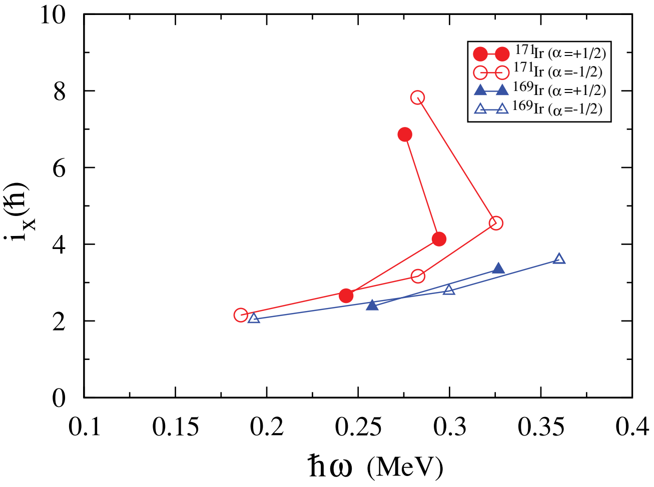

FIG. 9. (Color online) Experimental aligned angular momentum i_x as a function of rotational frequency $\hbar\omega$ for the $h_{11/2}$ band in ^{169}Ir and ^{171}Ir. The filled (open) symbols represent the $\alpha = +1/2$ ($\alpha = -1/2$) signature. The same Harris parameters $\mathfrak{J}_0 = 10\hbar^2$ MeV^{-1} and $\mathfrak{J}_1 = 50\hbar^4$ MeV^{-3} [15] have been used for both nuclides.

mixing of low-K components into the high-K $h_{11/2}$ proton configuration. Figure 8 shows that the signature splitting, as reflected by the staggering parameter, first increases rapidly as N decreases from ^{175}Ir to ^{171}Ir. The following increase from $N = 94$ (^{171}Ir) to $N = 92$ (^{169}Ir) is then significantly smaller. The iridium isotopes exhibit, at low spin ($I < 12\hbar$), the same trend of increasing signature splitting as in the odd-mass $^{167-173}$Re isotopes [34] with decreasing neutron number, indicating a general trend of increasing shape asymmetry as the closed neutron shell $N = 82$ is approached. Interestingly, these observations seem not to be consistent with the results of the TRS calculations, which predict the opposite trend, i.e., a less pronounced γ deformation as a function of decreasing neutron number in the range $N = 98 \rightarrow N = 92$.

The trend of signature splitting tailing off with increasing spin observed in heavier iridium isotopes (see Fig. 8) cannot be confirmed in ^{169}Ir, as Band 1 in Fig. 2 only extends to spin $I = 23/2$. It also does not extend to high enough spins for any sign of a paired $(\nu i_{13/2})^2$ band crossing to be visible as in $^{171-175}$Ir (see Fig. 9). In ^{169}Ir the characteristic "back-bending" for the alignment is not observed. The corresponding alignment plot for ^{171}Ir indicates for ^{169}Ir either a delay in the crossing frequency or a significant difference in the interaction strength between the 1qp band and the S-band. The former is an expected result of the lowering of the neutron Fermi level below the $i_{13/2}$ shell. CSM calculations predict this shift to be ∼50 keV. In addition, a reduced interaction strength for $N = 92$ as compared to $N = 94$ can delay the onset of the alignment. Differences in the shapes between the two isotopes may also affect the band crossing frequency. This is the same trend that can be observed in ^{169}Re and ^{167}Re [30,34], where the alignment is delayed by ∼50 keV to higher frequencies when the neutron number changes from $N = 94$ to $N = 92$.

Considering the γ-soft nature of these neutron-deficient nuclides it is still not clear whether the large values of the staggering parameter observed in ^{169}Ir and ^{171}Ir is evidence of a correspondingly large rigid triaxial deformation. Based on the increased experimental signature splitting as a function of decreasing neutron number in these isotopes, one would expect that this should reflect an increased shape asymmetry. This expectation is not confirmed by the TRS calculations. Notably, the calculated γ deformations of ^{169}Ir ($\gamma \approx -16^\circ$) and ^{175}Ir ($\gamma \approx -14^\circ$) [11] are roughly the same while at the same time the former exhibits an experimental signature splitting of ≃150 keV and the latter shows virtually no signature splitting at all. On the other hand the γ-softness of the calculated energy minima tends to increase with increasing neutron number as can be seen in Fig. 5. Taking this into account, the effective γ deformation may be different from that in a given minimum point. It is also noteworthy that although the signature splitting of the $h_{11/2}$ band is expected to be associated with a pronounced triaxial shape, CSM calculations show that such a large signature splitting is only expected for $\gamma < -40^\circ$ and that negligible signature splitting is predicted at the deformation $\gamma \approx -20^\circ$ [12]. Also, for ^{171}Ir [15] particle-rotor calculations using the predicted γ deformation obtained by TRS calculations ($\gamma \approx -20^\circ$) do not fully reproduce the observed signature splitting. The particle-rotor model calculation is also sensitive to the moment-of-inertia and Coriolis attenuation parameters in addition to its deformation parameters and is therefore not optimized for signature splitting estimates. Nevertheless, the observed band in ^{169}Ir is best described to be associated with a significant triaxial deformation and the predicted $h_{11/2}$ band head.

Additional light on the assigned $h_{11/2}$ configuration of the yrast band in ^{169}Ir can be shed with help of the deduced $B(M1; I \rightarrow I-1)/B(E2; I \rightarrow I-2)$ ratios, which are sensitive to the single-particle configuration as well as to the nuclear quadrupole deformation. Figure 10 displays a comparison of theoretical and experimental deduced $B(M1)/B(E2)$ values. Theoretical estimates are obtained through the semi-classical formalism of Dönau and Frauendorf [36,37]:

$$\begin{aligned}\frac{B(M1;I\to I-1)}{B(E2;I\to I-2)} &= \frac{12}{5Q_0^2\cos^2(\gamma+30^\circ)}\left[1-\frac{K^2}{(I-1/2)^2}\right]^{-2}\\ &\times\frac{K^2}{I^2}\left[1\pm\frac{\Delta e'}{\hbar\omega}\right]^2\{(g_1-g_R)[(I^2-K^2)^{1/2}-i_1]\\ &-(g_2-g_R)i_2\}^2\quad\left[\frac{\mu_N^2}{e^2\mathrm{b}^2}\right],\end{aligned}\tag{3}$$

where the $+(-)$ sign in the signature splitting term is for transitions from unfavored(favored) to favored(unfavored) signature. The expression takes into account the effect of the triaxiality parameter γ. The suffixes 1 and 2 refer to the strongly coupled and decoupled quasiparticles respectively. In this case, there is no decoupled particle present since the configuration only involves a single strongly coupled quasiproton. Also the alignment i_1 is set to zero. The single-particle gyro-magnetic g_1 factor was obtained through the Schmidt relation [38]

$$g_1 = g_l \pm \frac{1}{2l+1}(g_s-g_l)\quad\text{for}\quad j=l\pm\frac{1}{2},\tag{4}$$

where $g_l=1$ and $g_s=0.6g_s^{\text{free}}$ ($g_s^{\text{free}}=5.5856$) for the proton. The plus sign in Eq. (4) is for the $l+\frac{1}{2}$ $h_{11/2}$ proton orbital leading to a single-particle g-factor calculated to be $g_1=1.21$. The rotational gyromagnetic factor g_R was taken to be $Z/A=0.456$. A band head K-value of 11/2 was used and the quadrupole moment was set to $Q_0=5.6$ *e*b based on the TRS calculations. The ratio of the experimental reduced magnetic dipole [$B(M1)$] and stretched electric qudrupole [$B(E2)$] transition probabilities have been extracted using the formula [10]

$$\begin{aligned}\frac{B(M1;I\to I-1)}{B(E2;I\to I-2)} &= 0.697\frac{[E_\gamma(I\to I-2)]^5}{[E_\gamma(I\to I-1)]^3}\frac{1}{\lambda}\frac{1}{1+\delta^2}\quad\left[\frac{\mu_N^2}{e^2\mathrm{b}^2}\right],\end{aligned}\tag{5}$$

where the transition energies $E_\gamma(I\to I-1)$ and $E_\gamma(I\to I-2)$ are given in units of MeV and represent $\Delta I=1$ and $\Delta I=2$ transitions, respectively. The experimental γ-ray branching ratios λ are taken as the ratio of the measured γ-ray intensities of the $\Delta I=2$ and $\Delta I=1$ transitions defined as

$$\lambda = \frac{T_\gamma(I\to I-2)}{T_\gamma(I\to I-1)}.\tag{6}$$

The $E2/M1$ multipolarity mixing ratio δ deduced from angular-correlation coefficients in heavier odd-A iridium isotopes $^{171-173}$Ir have values $\delta<0.2$ [10,15]. Such small δ values would have negligible effect on the extracted $B(M1;I\to I-1)/B(E2;I\to I-2)$ values and therefore a constant mixing ratio of $\delta=0$ has been used in the analysis. Figure 10 supports the assumption of a one-quasiparticle proton residing in the [505]11/2$^-$ Nilsson orbital coupled to an even-even core of moderate quadrupole deformation $\beta_2=0.14$ with negative triaxiality parameter $\gamma=-16^\circ$. The theoretical $B(M1)/B(E2)$ values reproduce the experimentally deduced values with increasing spin even when the band head K-value at $K=11/2$ and the deformation parameters from the TRS calculation are left unchanged. Hence, no use of an effective K-value is necessary at the observed spins which otherwise could point to a decrease in K from the band-head K with increasing frequency and taken as evidence for K-mixing. Up to the observed spin $I^\pi=23/2^-$ in the yrast [505]11/2$^-$ band no smooth increase for the quadrupole moment, from the band-head value $Q_0=5.6$ *e*b used in the calculation, is needed in order to fit the experimental data points. With a higher γ value and similar β_2 deformation the theoretical values overestimate the strength of the $B(M1)/B(E2)$ ratios. Thus, the calculated values for the relevant $\pi h_{11/2}$ orbital are in good agreement with the assumed configuration and its calculated deformation parameters.

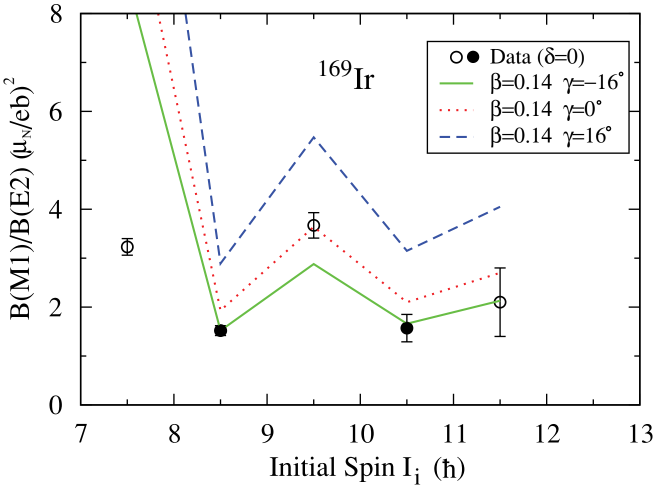

FIG. 10. (Color online) Experimental $B(M1;I\to I-1)/B(E2;I\to I-2)$ values as a function of initial spin I_i for the [505]11/2$^-$ band in ^{169}Ir. The measured values are compared with the predictions of the semiclassical model of Dönau and Frauendorf, shown here both for positive and negative γ deformation as described in the text. The slight staggering of the experimental values is due to favored ($\alpha=+1/2$) and unfavored ($\alpha=-1/2$) signature of the strongly-coupled band, represented by filled and open symbols, respectively. A γ deformation of $\gamma\approx-16^\circ$ agrees best to the data.

V. SUMMARY

Gamma-ray transitions have for the first time been assigned to the neutron-deficient nucleus ^{169}Ir using the recoil-decay tagging technique. A level structure has been established comprising one yrast coupled band based on the α-decaying 11/2$^-$ state, and several other bands feeding into it. The yrast structure has been assigned a single-quasiproton configuration based on the [505]11/2$^-$ Nilsson state of $h_{11/2}$ shell model parentage. This state is predicted by TRS calculations to have a small prolate deformation of $\beta_2=0.14$ and to possess a triaxial shape with $\gamma=-16^\circ$. This prediction is in agreement with the deduced $B(M1)/B(E2)$ ratios. The trend of increasing signature splitting in the $h_{11/2}$ bands of the light iridium isotopes as a function decreasing neutron number is carried through into ^{169}Ir. This experimental trend is, however, not consistent with the TRS calculations which predict an opposite trend in shape asymmetry. On the other hand, the softness of the predicted shapes adds complexity to the interpretation of these results.

ACKNOWLEDGMENTS

The authors wish to extend their thanks to the crew at the Accelerator Laboratory at the University of Jyväskylä for their excellent technical support. Further support for this work has been provided by the Swedish Research Council, the Academy of Finland under the Finnish Center of Excellence Programme 2000–2005 (Project No. 44875, Nuclear and Condensed Matter Physics Programme at JYFL), the U.K. Engineering and Physical Sciences Research Council and the European Union Fifth Framework Programme "Improving Human Potential—Access to Research Infrastructure" (Contract No. HPRI-CT-1999-00044) and the Turkish Atomic Energy Authority (TAEK) under project No. OUK 120100-4. We also thank the U.K./France (EPSRC/IN2P3) detector Loan Pool and EUROBALL owners committee (γ-pool network) for the EUROGAM detectors of JUROGAM. M.S., J.P., and K.V. de V. would like to acknowledge the support through the European Community Marie Curie programme.

[1] J. L. Wood *et al.*, Phys. Rep. **215**, 101 (1992).
[2] G. D. Dracoulis *et al.*, J. Phys. G **12**, L97 (1986).
[3] B. Cederwall *et al.*, Z. Phys. A **337**, 283 (1990).
[4] G. D. Dracoulis *et al.*, Phys. Rev. C **44**, R1246 (1991).
[5] P. M. Davidson *et al.*, Nucl. Phys. **A568**, 90 (1994).
[6] D. T. Joss *et al.*, Nucl. Phys. **A689**, 631 (2001).
[7] R. D. Page *et al.*, Phys. Rev. C **53**, 660 (1996).
[8] J. Meyer-Ter-Vehn, Nucl. Phys. **A249**, 111 (1975); **A249**, 141 (1975).
[9] R. Sahu, M. Satpathy, and L. Satpathy, Phys. Rev. C **23**, 1777 (1981).
[10] S. Juutinen *et al.*, Nucl. Phys. **A526**, 346 (1991).
[11] B. Cederwall *et al.*, Phys. Rev. C **43**, R2031 (1991).
[12] G. D. Dracoulis *et al.*, Nucl. Phys. **A534**, 173 (1991).
[13] H.-Q. Jin *et al.*, Phys. Rev. C **53**, 2106 (1996).
[14] U. Garg *et al.*, Phys. Lett. **B151**, 335 (1985).
[15] R. A. Bark *et al.*, Nucl. Phys. **A657**, 113 (1999).
[16] G. L. Poli *et al.*, Phys. Rev. C **59**, R2979 (1999).
[17] C. W. Beausang *et al.*, Nucl. Instrum. Methods A **313**, 37 (1992).
[18] C. R. Alvarez *et al.*, Nucl. Phys. News **3**(3), 10 (1993).
[19] M. Leino *et al.*, Nucl. Instrum. Methods B **99**, 653 (1995).
[20] M. Leino, Nucl. Instrum. Methods B **126**, 320 (1997).
[21] R. D. Page *et al.*, Nucl. Instrum. Methods Phys. Res. B **204**, 634 (2003).
[22] I. H. Lazarus *et al.*, IEEE Trans. Nucl. Sci. **48**, 567 (2001).
[23] P. Rahkila, Slide report of Midwinter workshop on tagging methods and experiments, Jyväskylä, (2004).
[24] E. S. Paul *et al.*, Phys. Rev. C **51**, 78 (1995).
[25] R. S. Simon *et al.*, Z. Phys. A **325**, 197 (1986).
[26] D. T. Joss *et al.*, Phys. Rev. C **74**, 014302 (2006).
[27] D. C. Radford *et al.*, Nucl. Instrum. Methods A **361**, 297 (1995).
[28] B. Hadinia *et al.* (to be published).
[29] G. D. Dracoulis *et al.*, Nucl. Phys. **A486**, 414 (1988).
[30] X. H. Zhou *et al.*, Eur. Phys. J. A **19**, 11 (2004).
[31] W. Nazarewicz *et al.*, Nucl. Phys. **A435**, 397 (1985).
[32] R. Wyss *et al.*, Nucl. Phys. **A503**, 244 (1989).
[33] R. Wyss *et al.*, Phys. Lett. **B215**, 211 (1988).
[34] D. T. Joss *et al.*, Phys. Rev. C **68**, 014303 (2003).
[35] I. Hamamoto, Phys. Lett. **B211**, 1 (1988).
[36] D. Dönau and S. Frauendorf, in *Proceedings of the Conference on High Angular Momentum Properties of Nuclei, Oak Ridge*, edited by N. R. Johnson (Harwood, New York, 1983), p. 143.
[37] F. Dönau *et al.*, Nucl. Phys. **A471**, 469 (1987).
[38] K. L. G. Heyde, *The Nuclear Shell Model* (Springer-Verlag, Berlin Heidelberg, 1994), p. 174.